

Large-stroke piezo-actuated planar motor for nanopositioning applications

Junbin Zhang¹, Yanran Ding¹, Junjie Shen¹, Hui Zou¹ and Peisen S. Huang^{1,2}

¹University of Michigan – Shanghai Jiao Tong University Joint Institute, Shanghai, P.R.China

²State Key Laboratory of Mechanical Systems and Vibration, Shanghai, P.R.China

Corresponding author: Junbin Zhang

E-mail addresses: zhangjunbin.max@gmail.com (Junbin Zhang)

Tel.: +86 18621666904

Postal address: Room 115, University of Michigan – Shanghai Jiao Tong University Joint Institute, Shanghai Jiao Tong University, Dong Chuan Road, Shanghai, China

E-mail addresses of Other Authors: dingyanran.hi@gmail.com (Yanran Ding), juejie.shen@sjtu.edu.cn (Junjie Shen), Zouhui@sjtu.edu.cn (Hui Zou), peisen.huang@sjtu.edu.cn (Peisen S. Huang)

Abstract

This paper presents a large-stroke piezo-actuated planar motor for nano-positioning applications. The planar motor uses an air bearing with vacuum preload to reduce friction in motion directions. Four piezo legs located at each corner of the mover can perform three operation modes to drive the planar motor: the skiing mode, the stepping mode, and the tilting mode. The skiing mode is a high-speed actuation mode. The stepping mode provides high-resolution trajectory tracking capability. The tilting mode allows for fine adjustment of the stage in its final position with the highest resolution. These three operation modes have different positioning advantages and can be combined to achieve both a high positioning speed and a high positioning resolution. The piezo-actuated planar motor has large stroke that is only limited by the base size and large rotation range up to 360°. An active planar encoder based on flat panel display has been developed as a feedback system to evaluate the motion performance of the planar motor including motion resolution, maximum motion speed and trajectory tracking accuracy.

Keywords

planar motor, stage, positioning system, piezo, flexure hinge, planar encoder, semiconductor production

1. Introduction

High precision planar motion systems are widely used in modern industrial and scientific applications, such as semiconductor manufacturing, precision machining, etc. [1-5]. Many of these applications require sub-micron to nanometer positioning resolution and accuracy as well as a large range of motion. Conventional multi-degrees-of-freedom (multi-DOF) stages are constructed by stacking multiple single-DOF stages together, which are relatively easy to construct and control. However, such stages are typically too bulky for fast motion response. They are also prone to errors due to error accumulation and misalignment between motion axes [6,7].

To overcome the above drawbacks of conventional multi-DOF stages, a new type of stage named as planar motor has been developed. Various planar motor systems include electromagnetic planar motors [8-11], ultra-

sonic planar motors [12-14], piezo-walking positioning stage [15-16], and stick-slip planar motion stages [17-18]. These planar motor systems each have only one mover. The single mover is actuated directly by driving forces to perform multi-DOF motion. Therefore, they do not have the drawbacks of the conventional stacking motion systems. However, they also have their own shortcomings. Electromagnetic planar motors require complex dynamic motion control. Ultrasonic planar motors require complex dynamic analysis of the multi-DOF ultrasonic motor (USM) and are still immature for real applications. Piezo-walking positioning stage uses the two groups of piezo legs to actuate the planar motor step by step, which is similar to walking, however the motion speed is limited. Stages based on the stick-slip effect have a limited frictional driving force and suffer from severe wear due to the existence of slip.

To overcome some of the drawbacks of the planar motor systems described above, a novel large-stroke piezo-actuated planar motor for nano-positioning is proposed [19]. The planar motor uses an air bearing with vacuum preload to reduce friction in the direction of motion while maintaining high stiffness in the direction perpendicular to air bearing surface. Two types of piezo legs are used to drive the planar motor including two 1-DOF piezo legs and two 3-DOF piezo legs. The planar motor can operate in three modes: the skiing mode, the stepping mode, and the tilting mode. The skiing mode is a high-speed actuation mode for large distance adjustment. The stepping mode provides high-resolution positioning capability for trajectory tracking application. The tilting mode adjusts the planar motor in 6-DOF with nanometer resolution in translational direction and sub-arcsec resolution in angular direction. The above three operation modes can also be combined to drive the planar motor in a high positioning speed and a high positioning resolution with omni-directional motility. The motion range of the proposed planar motor is only limited by the size of the base and the rotation range is up to 360° . Because of the natural high stiffness of the piezoelectric actuator, the stage has an excellent capability to resist external vibration when four piezo legs clamp to the base. The large motion range and high motion resolution of the planar motor require the feedback system to have the same features. Therefore, an active planar encoder with large linear and angular measurement range is developed to evaluate the trajectory tracking performance of the planar motor. Another system setup uses the laser interferometer to test the motion resolution of the planar motor.

This paper describes the working principle of the large-stroke piezo-actuated planar motor and the active planar encoder specifically designed for feedback control. Experimental data for demonstrating the motion performance of the planar motor is presented.

2. Mechanical design of planar motor

As shown in Fig. 1(a), the proposed planar motor has four piezo legs located at each corner of the mover. The size of the mover is 120×120 mm. A vacuum preloaded air bearing is positioned in the center, which provides a supporting and clamping force for the mover. Pitch and roll angles of the mover platform can be adjusted by three micro adjustment screws evenly distributed around a flexure hinge. The flexure hinge connects the air bearing and the mover. Two 3-DOF piezo legs, each providing XYZ motion at the tip of the leg, are mounted at two diagonally opposite corners. Two 1-DOF piezo legs providing Z motion control are mounted at the other two corners. The planar motor has three DOFs ($XY\theta_z$) and omni-directional motility with four piezo legs operating cooperatively under different operation modes.

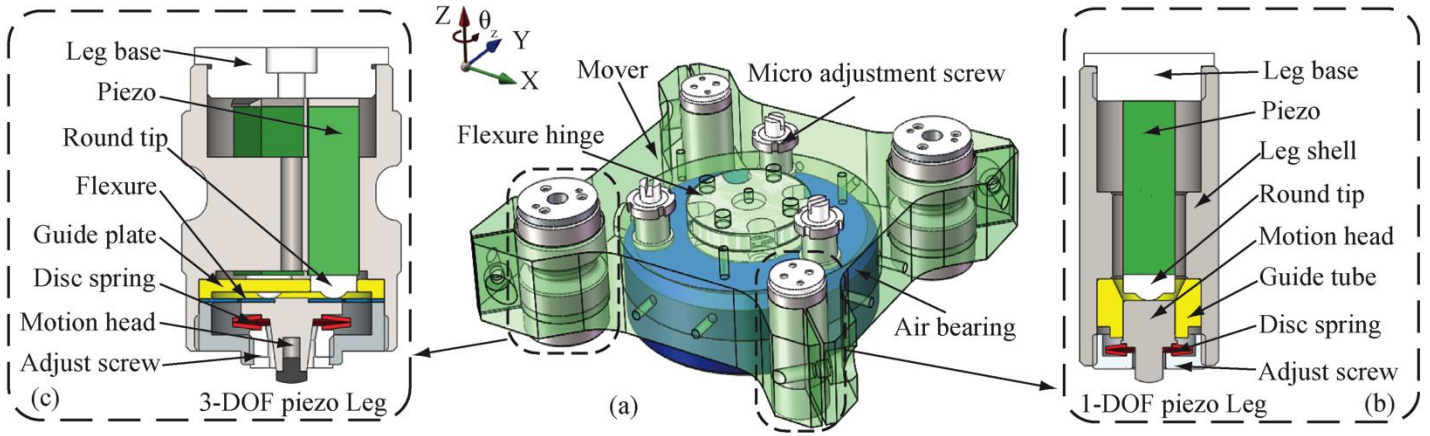


Fig. 1. Design of the piezo-actuated planar motor (a) Overall design (b) Mechanical design of 1-DOF piezo leg (c) Mechanical design of 3-DOF piezo leg.

Fig. 1(b) shows the mechanical design of the 1-DOF piezo leg, which provides linear motion in Z direction. A piezo-actuator with a displacement range of $15\ \mu\text{m}$ is assembled in the leg. Two disc springs provide the adjustable preload force on the motion head. A round tip is mounted between the piezo-actuator and the motion head to prevent any shear or torque force acting on the piezo-actuator. When the piezo-actuator extends, the tip of the motion head will contact with the base, providing the braking effect. Fig. 1(c) shows the mechanical design of the 3-DOF piezo leg. Three piezo-actuators, each with a round tip, are mounted inside the leg. A guide plate provides three round holes as guidance for three round tips, which are distributed evenly along a circle of $5\ \text{mm}$ radius. Two disc springs are stacked together to provide a large preload force for high-speed motion of the motion head. The motion head consists of two components, the main body made by lightweight aluminum and the tip made by wear-resistant material. A specially designed flexure fixed on the motion head has low stiffness in $\theta_x\theta_yZ$ directions and high stiffness in $XY\theta_z$ directions. Therefore when three piezo-actuators extend, the motion head only moves in three DOFs ($\theta_x\theta_yZ$), which provide driving force for the planar motor in X and Y directions at the tip of the motion head. Fig. 2(a) and Fig. 2(b) show simulation results of the structural deformations with an external force of $1\ \text{N}$ applied in X and Z directions. The results show that the structural stiffness of the flexure in X and Y directions is 100 times larger than that in Z direction. In Fig. 2(c), the motion simulation result of the motion head with three inputs from piezo-actuators shows that the tip of the motion head moves in an elliptic trajectory. Fig. 3 shows the prototype of piezo legs and the assembled planar motor.

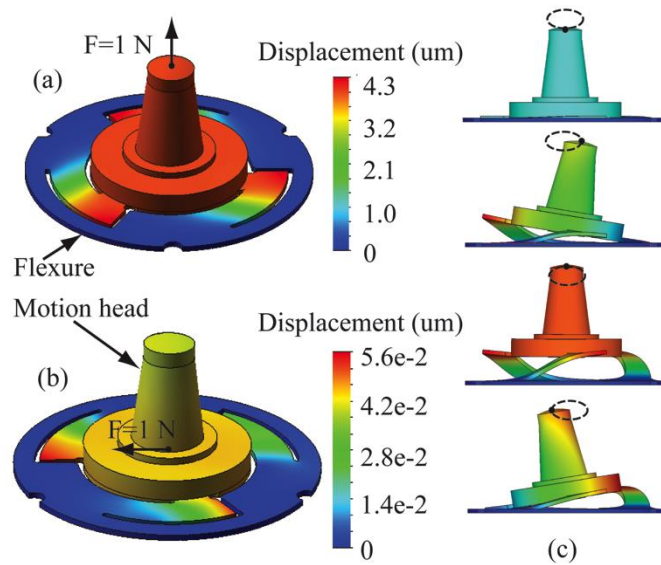


Fig. 2. Structural simulation results of the flexure fixed with the motion head. (a) Z-direction displacement under a force of 1N. (b) X-direction displacement under a force of 1N. (c) Motion simulation result of the motion head magnified by 200 times.

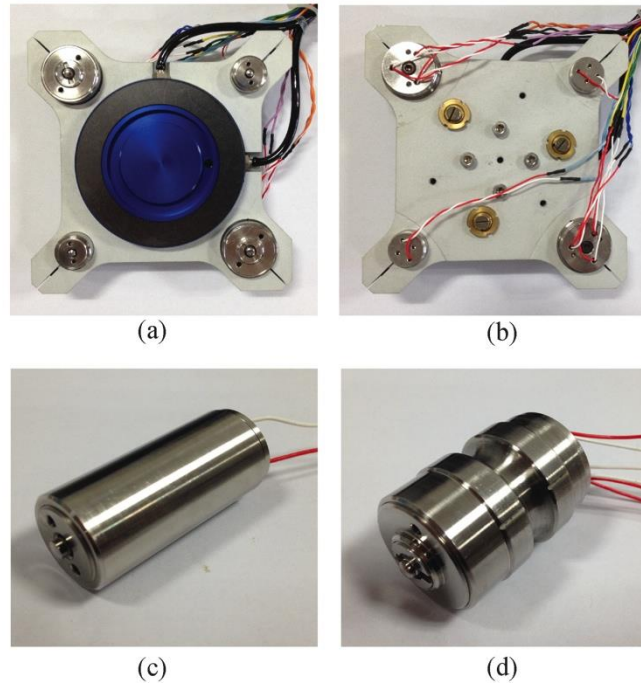


Fig. 3. Photos of the planar motor. (a) Bottom view. (b) Top view. (c) 1-DOF piezo leg. (d) 3-DOF piezo leg.

3. THREE OPERATION MODES

With the four piezo legs working cooperatively, the planar motor can operate under three different operation modes: the skiing mode, the stepping mode, and the tilting mode (Fig. 4). In the skiing mode, the two 3-DOF piezo legs move like ski sticks in high frequency to drive the planar motor while the two 1-DOF piezo legs are retracted and not used. Due to the frictionless condition provided by the air bearing, the planar motor can move in high speed under this mode. In order to reduce the slippage in this mode, the acceleration of the planar motor must be controlled within a range to keep the actuation force less than the maximum static friction force. In the

stepping mode, the planar motor moves step by step in a low frequency. When the 3-DOF piezo legs extend to drive the mover, the 1-DOF piezo legs are retracted. When the 3-DOF piezo legs are retracted to step forward, the 1-DOF piezo legs extend to clamp on the base. Due to the continuous contact between the legs and the base, the stepping mode provides more accurate position control compared to the skiing mode. In the tilting mode, all four legs clamp on the base. The mover can achieve fine position adjustment in 6-DOF through the tilting of the motion head of the 3-DOF piezo legs and extension/contraction of the 1-DOF piezo legs. This operation mode provides the most stable and highest resolution position control. It can be used for mask alignment in the stepper system before the photolithography exposure process starts. The above three operation modes can also be combined to achieve both speed and accuracy in position control.

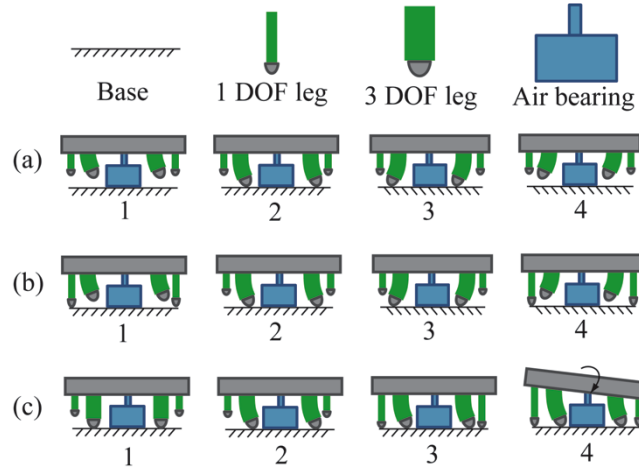


Fig. 4. Three operation modes. (a) Skiing mode. (b) Stepping mode. (c) Tilting mode.

4. MOTION CONTROL

The control algorithms of the four piezo legs under three operation modes are discussed in this section. Fig. 5 shows the definition of the four coordinate systems, O_b , O_m , O_{leg_1} and O_{leg_2} , which are attached to the base, mover, 1st, and 2nd 3-DOF piezo legs respectively. The coordinate systems of the 3-DOF piezo legs and the mover have the same X - and Y -axes directions. Assume that the desired velocity of the mover with respect to the base coordinate system O_b is:

$$\mathbf{V}_m^b = [\dot{x}_m^b \quad \dot{y}_m^b \quad \dot{\theta}_z]^T \quad (1)$$

Given the current angular position θ_z of the mover, the desired velocity of the i th 3-DOF piezo leg with respect to its own coordinate system is:

$$\mathbf{V}_i^i = \mathbf{J}_i(\theta_z) \mathbf{V}_m^b, i = 1, 2 \quad (2)$$

where the Jacobian is:

$$\mathbf{J}_i(\theta_z) = \begin{bmatrix} \cos \theta_z & \sin \theta_z & -y_i^m \\ -\sin \theta_z & \cos \theta_z & x_i^m \end{bmatrix} \quad i = 1, 2 \quad (3)$$

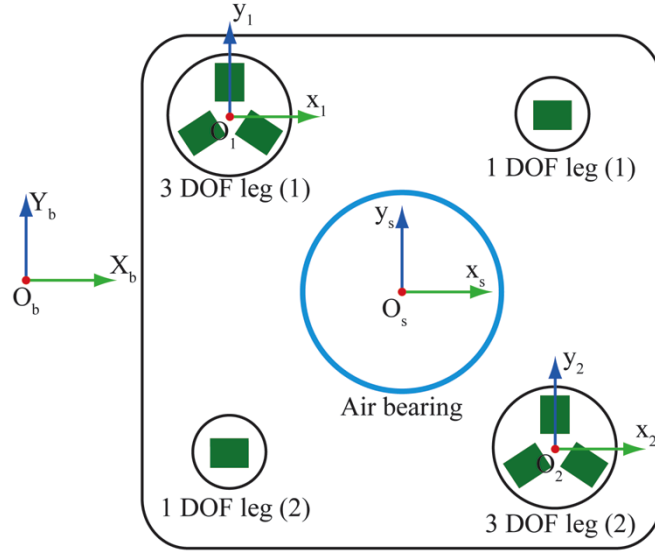


Fig. 5. Definition of the coordinate systems.

In the i th 3-DOF piezo leg, three piezo-actuators distributed evenly along a circle with radius of $r = 5$ mm, drive the motion head to provide 3-DOF motions (δ_i , Φ_i , and Z_i) as shown in Fig. 6. Two coordinate systems $O_{leg,i}$ and $O_{motion,i}$ are defined as follow. The leg coordinate system $O_{leg,i}$ is attached to the base of the i th 3-DOF piezo leg, whose XY plane coincides with the leg base and its origin is defined at the center of the leg base. The $Y_{leg,i}$ -axis coincides with the center of the 1st piezo-actuator while $Z_{leg,i}$ -axis is perpendicular to the leg base. The motion plane coordinate system $O_{motion,i}$ is defined such that the motion head rotates in its YZ plane (i.e. motion plane in pink color) and $Y_{motion,i}$ -axis is pointing at the desired motion direction of the leg. $Z_{motion,i}$ -axis aligns with $Z_{leg,i}$ -axis. The origin $O_{motion,i}$ coincides with the center of the top surface of the motion head only when all displacements of the three piezo-actuators are zero. The angle δ_i is defined as a right-handed rotation angle from $Y_{motion,i}$ -axis to $Y_{leg,i}$ -axis about $Z_{motion,i}$ -axis and is determined by the velocity vector V_i^l in Eq. (2). Rotation angle Φ_i and linear displacement Z_i define the motion trajectory of the motion head in the motion plane. The distance between the tip and the center of the top surface of the motion head is D . Given the three motion parameters (δ_i , Φ_i , and Z_i), the displacement of the j th piezo-actuator in the i th 3-DOF piezo leg can be obtained as:

$$d_{ji_3DOF} = -Z_i - r \cos[120^\circ(j-1) + \delta_i] \Phi_i \quad j = 1,2,3 \quad i = 1,2 \quad (4)$$

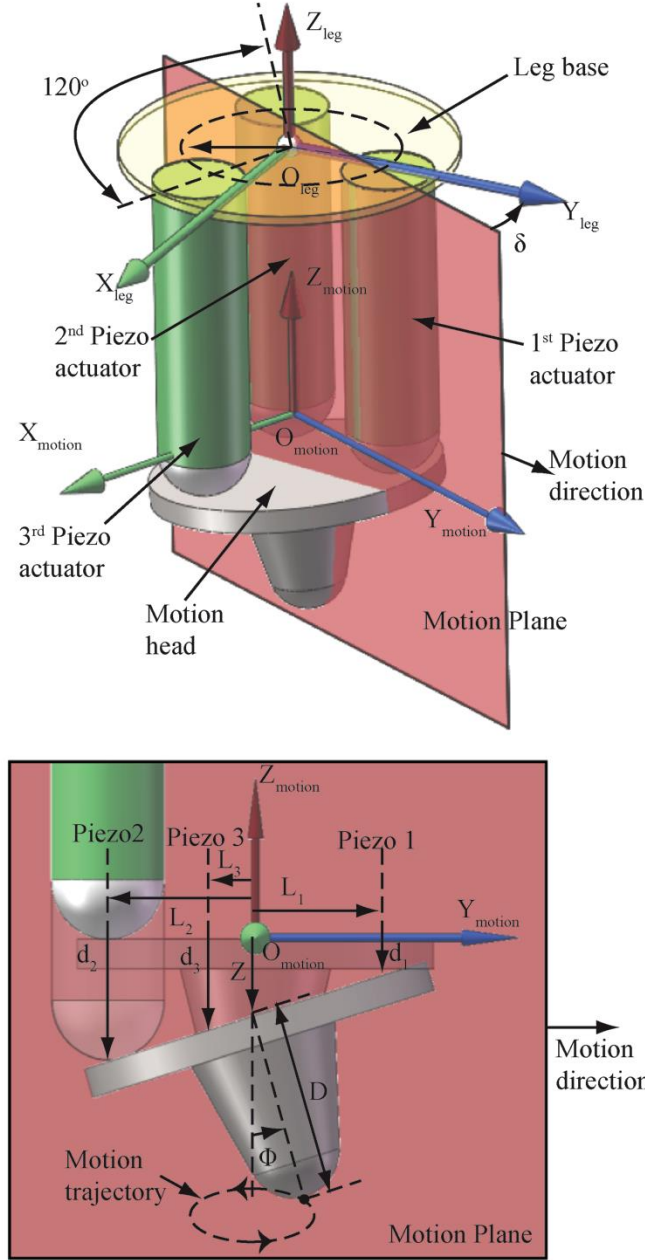


Fig. 6. Definition of parameters and coordinate systems of the 3-DOF piezo leg.

In the skiing mode, the tip of i th 3-DOF piezo leg moves along an elliptic trajectory repetitively in high frequency to drive the mover in high speed. The elliptic trajectory in Fig. 6 is defined with step height A_{z_i} and maximum swing angle A_{ϕ_i} . Given the motion frequency f and speed coefficient K_{ϕ} , we can derive the motion of each piezo-actuator as:

$$d_{ji_3DOF} = A_{ji} \cos(2\pi ft + \theta_{ji}) \quad j = 1, 2, 3 \quad i = 1, 2 \quad (5)$$

where

$$A_{ji} = \sqrt{r^2 \cos^2[120^\circ(j-1) + \text{atan2}(\mathbf{V}_i^i)] A_{\phi_i}^2 + A_{z_i}^2} \quad (6)$$

$$\theta_{ji} = \text{atan2}\{-A_{z_i}, -r \cos[120^\circ(j-1) + \text{atan2}(\mathbf{V}_i^i)] A_{\phi_i}\} \quad (7)$$

$$A_{\phi_i} = \frac{|V_i^i|}{fK_{\phi}} \quad (8)$$

In the stepping mode, all four piezo legs work cooperatively to drive the mover step by step. The control of the 3-DOF piezo legs is the same as that in the skiing mode but with a relatively low driving frequency (less than 50 Hz). The motion of the 1-DOF piezo legs has a phase difference of π compared to the Z displacement of the motion head in 3-DOF piezo legs, which means that the 1-DOF piezo legs can extend to clamp the mover when the 3-DOF piezo legs are lifted up. When the extension displacement A_i is given, the motion equation of the i th 1-DOF piezo legs is evaluated as:

$$d_{i_1DOF} = A_i \cdot \cos\left(2\pi ft - \frac{\pi}{2}\right) \quad i = 1,2 \quad (9)$$

In the tilting mode, the 3-DOF and 1-DOF piezo legs tilt, extend, or contract to fine adjust the position of the planar motor in 6-DOF. The motion range of tilting mode is limited to the working range of the piezo-actuator, which only suits for the small range adjustment to the target position. Given the desired position adjustment vectors $\Delta P1_m^b$ and $\Delta P2_m^b$, the displacement of the j th piezo-actuator in i th 3-DOF piezo leg and piezo-actuator in i th 1-DOF piezo leg can be derived as:

$$d_{i_1DOF} = [1 \quad y_{i_1DOF}^m \quad -x_{i_1DOF}^m] \Delta P2_s^b \quad i = 1,2 \quad (10)$$

$$d_{ji_3DOF} = -Z_i - r \cos[120^\circ(j-1) + \delta_i] \Delta \Phi_i \quad j = 1,2,3 \quad i = 1,2 \quad (11)$$

where

$$\Delta P1_m^b = [\Delta x_m^b \quad \Delta y_m^b \quad \Delta \theta_z]^T \quad (12)$$

$$\Delta P2_m^b = [\Delta z_m^b \quad \Delta \theta_x \quad \Delta \theta_y]^T \quad (13)$$

$$\delta_i = \text{atan2}[J_i(\theta_z) \Delta P1_m^b] \quad (14)$$

$$\Delta \Phi_i = -|J_i(\theta_z) \Delta P1_m^b|/D \quad (15)$$

$$Z_i = [1 \quad y_{i_3DOF}^m \quad -x_{i_3DOF}^m] \Delta P2_m^b \quad (16)$$

The control diagram of the planar motor system is shown in Fig. 7. The host PC obtains the sensor signal from the position encoder and calculates the current position of the planar motor. The current position is used in motion trajectory planning to generate the next target position. The user can manually select one of the three operation modes to actuate the planar motor. Besides the user can also select an automated mode, in which the motion-planning unit can automatically choose the appropriate operation mode depending on the accuracy requirement and the distance between target and current position. Each operation mode has its own PID controller and the PID controllers generate the motion parameters: the mover velocity V_m^b under the skiing/stepping mode; or position adjustment $\Delta P1_m^b$ and $\Delta P2_m^b$ under the tilting mode. The control algorithms use the motion parameters to generate eight piezo-actuator control signals d_{i_1DOF} and d_{ji_3DOF} using FPGA control card. The piezo-actuator control signals are magnified by power amplifiers and sent to four piezo legs to actuate the planar motor. A graphic user interface (GUI) is available with various control inputs and position information.

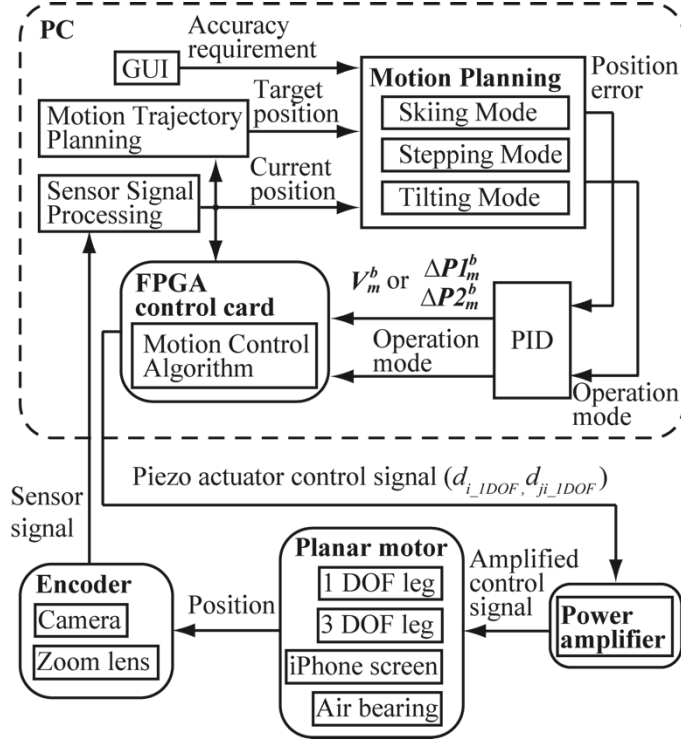


Fig. 7. Control diagram of the planar motor system.

5. ACTIVE PLANAR ENCODER

For closed-loop motion control of the planar motor, a multi-DOF position encoder is necessary to provide position feedback. However, the commercial measurement systems such as grid encoder and laser interferometer are unable to measure large angular displacement. In this research a novel large-range active planar encoder based on flat panel display has been developed to evaluate the position control performance of the planar motor in a large range of motion. Fig.8 shows the experimental setup. This encoder uses two 640×480 cameras, each with a compact low-distortion 1x lens. An iPhone 4S mounted on top of the mover is programmed to display two perpendicular sinusoidal fringe patterns with a pitch of 0.78 mm. Each camera captures different fringe images on the iPhone screen. Three sinusoidal signals $X1$, $X2$, and $Y1$ are obtained from three scanning areas of the two captured images, as shown in Fig. 8(b) and 8(c). The accurate phase of the center position of each sinusoidal signal is calculated using the fast Fourier transform (FFT) algorithm. The phase of the sinusoid signal changes periodically when the planar motor moves. Therefore, a phase unwrapping algorithm is used to convert the phase into a continuous signal. Three continuous phase signals are multiplied by a coefficient $0.78/2\pi$ to change into position information P_{X1} , P_{X2} and P_{Y1} . Fig. 9 shows the coordinate systems definition of planar encoder. In this system setup, the camera system is static while the display mounted on the planar motor is moving. Therefore, the display coordinate O_d is defined to coincide with the mover coordinate O_m . With kinematic transformation, the position parameters ($XY\theta_z$) of the mover with respect to the 1st camera coordinate system O_{c1} are calculated as:

$$\begin{bmatrix} X^{C1} \\ Y^{C1} \\ \theta_z \end{bmatrix} = -R_z(-\theta_z) \begin{bmatrix} \frac{P_{X1} + P_{X2}}{2} \\ P_{Y1} - \sin(\theta_z)X_{C1C2}^{C1} - \cos(\theta_z)Y_{C1C2}^{C1} \\ \arcsin\left(\frac{P_{X2} - P_{X1}}{L}\right) \end{bmatrix} \quad (17)$$

where $R_z(\theta)$ is the rotation matrix about Z -axis, X_{C1C2}^{C1} and Y_{C1C2}^{C1} are the position parameters between camera coordinates O_{C1} and O_{C2} . L is the distance between $X1$ and $X2$ scanning area. X_{C1C2}^{C1} , Y_{C1C2}^{C1} and L can be calculated by calibration. The camera system can obtain the absolute position of the mover by switching the sinusoidal fringe image to the coding image. The linear measurement range of this encoder depends only on the display size. The rotation measurement range is up to $\pm 45^\circ$, but can be extended to $\pm 180^\circ$ if the two fringe patterns on the screen is switched dynamically. The linear measurement resolutions along X - and Y -axes are 50 nm and 500 nm respectively and the measurement accuracy in a range of 40 mm is $\pm 0.6 \mu\text{m}$. The angular measurement resolution of θ_z is 2.2 arcsec. In the future, a large thin OLED display will be assembled on the top of the base and the camera system will be mounted on the planar motor to capture the fringe. Therefore, the future design can have a larger measurement range.

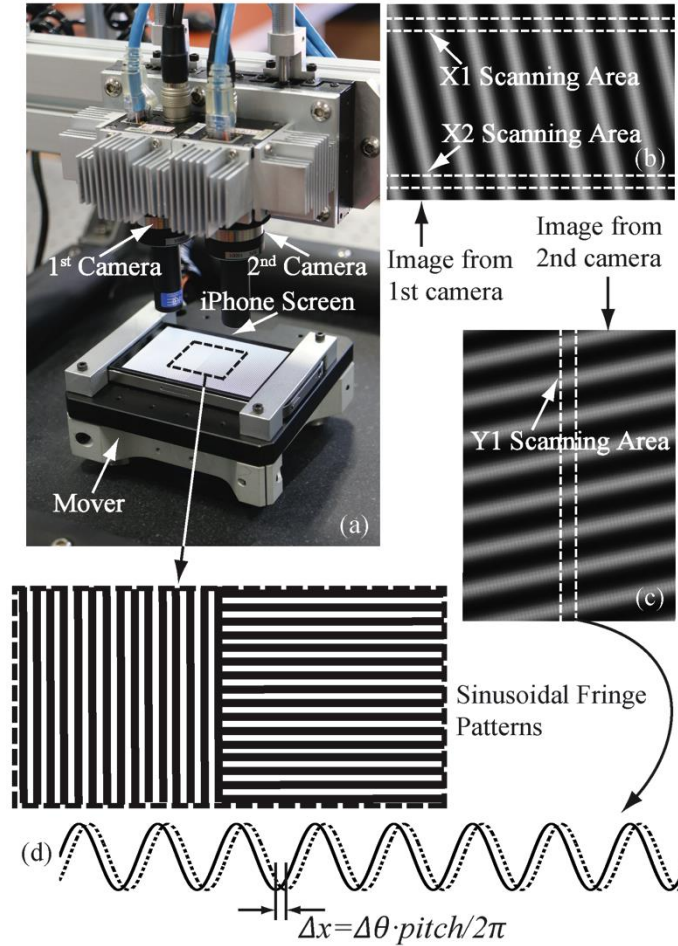


Fig. 8. System design of the active planar encoder (a) Planar motor integrated with the planar encoder. (b) $X1$ and $X2$ scanning area for calculating P_{X1} and P_{X2} . (c) $Y1$ scanning area for calculating P_{Y1} . (d) Converting the phase difference into displacement information.

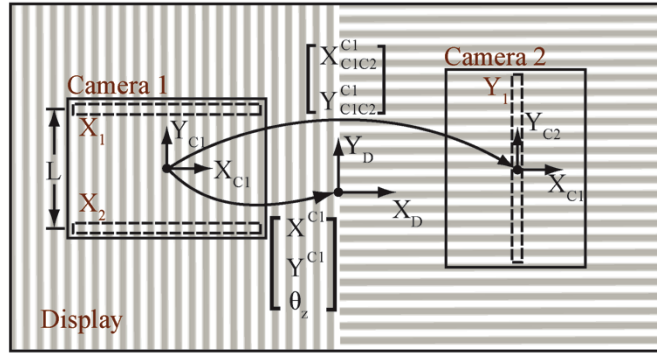


Fig. 9. Coordinate systems definition of the active planar encoder.

6. EXPERIMENTAL RESULTS

Four experiments were conducted to test the performance of the three operation modes of the planar motor.

The static stiffness of the planar motor under the tilting mode was tested using a tension meter, as shown in Fig. 10(a). The result shows that the planar motor has a static stiffness of 1.33 N/ μm when four piezo legs extend to brake the mover. Fig. 10(b) shows the mover clamped to the erected base without falling down, which demonstrates that the planar motor has a large static clamping force.

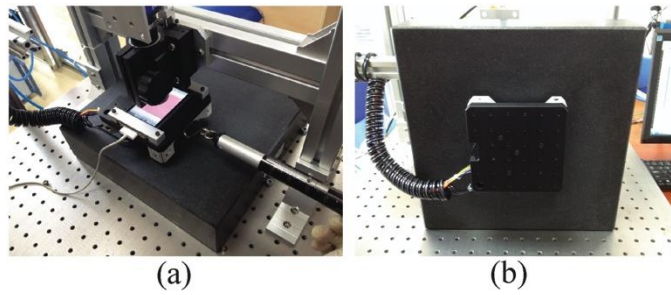


Fig.10. Static stiffness and clamping force tests. (a) Stiffness test. (b) Clamping force test.

The positioning resolution of the planar motor under the tilting mode was tested using a laser interferometer. Fig. 11(a) shows a 5 nm step test along the X -axis under the tilting mode. The standard deviation of the step test result is approximately 0.2 nm, which is the resolution limit of the laser interferometer. Fig. 11(b) shows a rotation test about the Z -axis with step size of 0.02 arcsec. The standard deviation of the rotation test result is approximately 0.001 arcsec. This experiment demonstrates the high positioning resolution of the planar motor under the tilting mode.

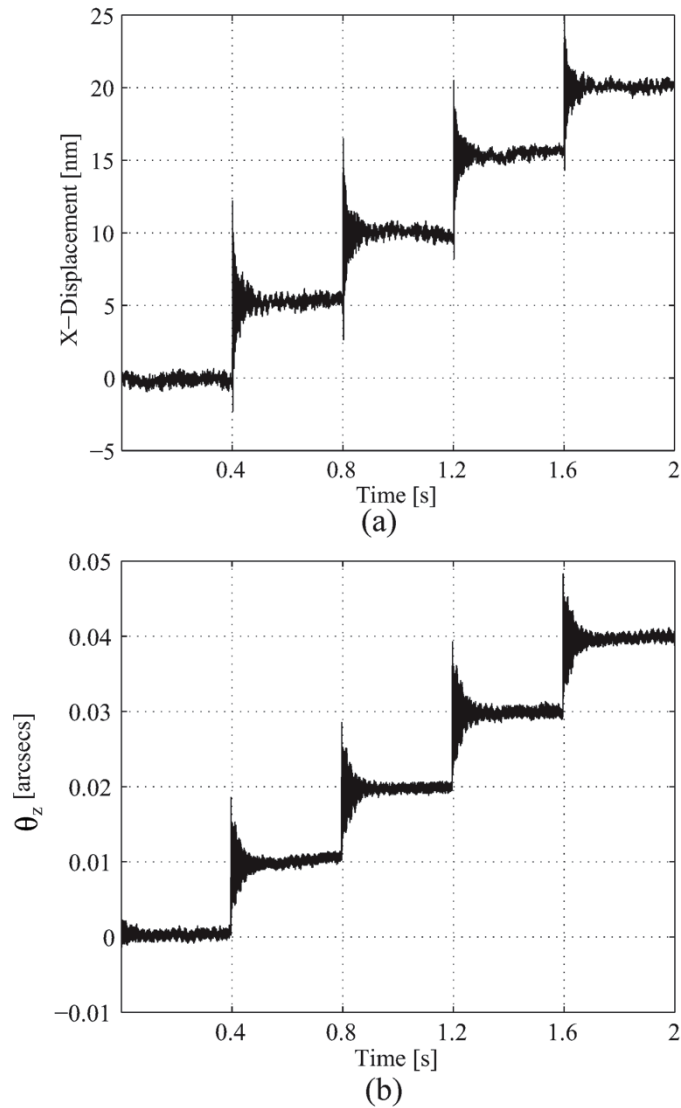
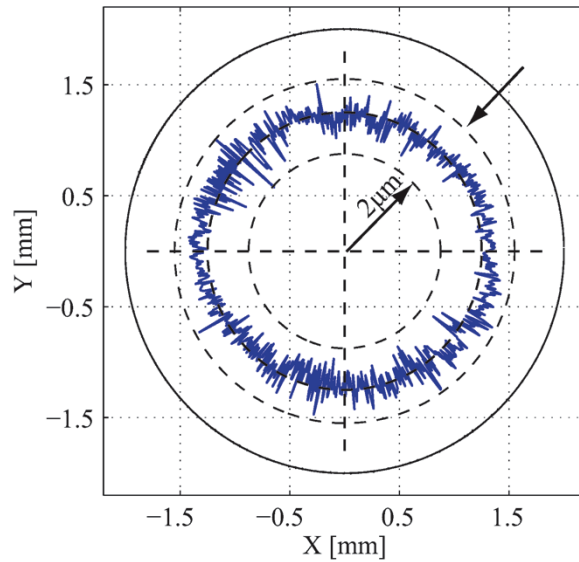
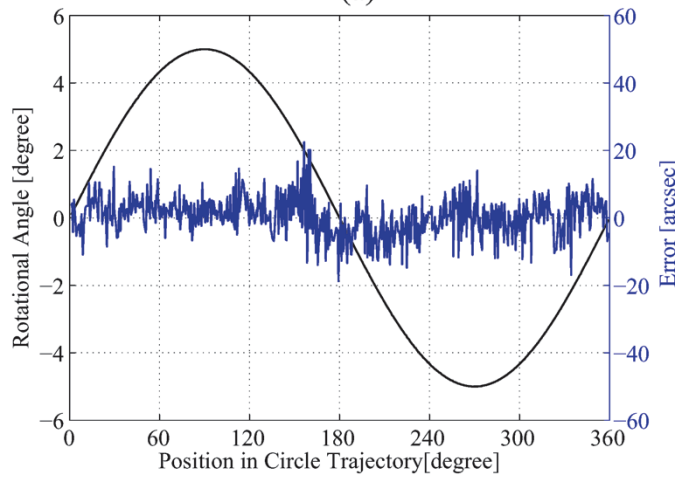


Fig.11. Tilting mode tests using a laser interferometer. (a) 5 nm step test along X -axis. (b) 0.02 arcsec step test about Z -axis.

The second experimental setup with an active planar encoder was used to evaluate the position control performance of the planar motor. The planar motor was controlled under the stepping mode to follow a special motion trajectory with the linear position of the mover following a circle with a radius of 2 mm, and in the meantime, the angular position θ_z following a sinusoidal curve with amplitude of 5° . The result of this tracking test in Fig. 12 shows the peak-to-peak deviation of the circular motion is approximately $\pm 1 \mu\text{m}$; the peak-to-peak deviation of the rotational motion is approximately ± 20 arcsec. The deviation of the motion result is comparable to the measurement resolution of the active planar encoder, so the tracking performance is limited to this planar encoder. This test demonstrates the omni-directional mobility and accurate trajectory tracking performance of the planar motor.



(a)



(b)

Fig.12. Large-range motion performance (a) Position trajectory with a radius of 2 mm. (b) Angular trajectory with a sinusoidal curve of 5° amplitude.

The motion speed test under the skiing mode was tested using active planar encoder as the feedback system. The speed of the planar motor can be adjusted by changing the driving frequency and the step size of the 3-DOF piezo legs. Fig. 13 shows the relationship between the driving frequency and the planar motor speed for different step sizes. Obviously, a larger step size and a higher driving frequency can drive the planar motor in a higher speed.

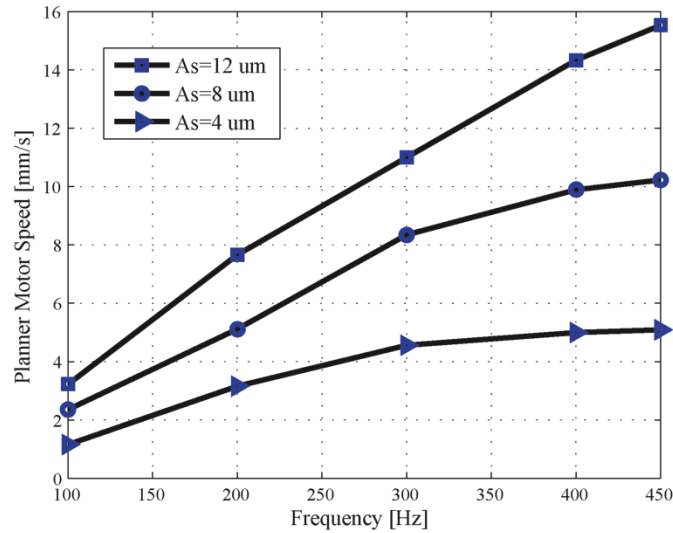


Fig. 13. Planar motor speed vs. driving frequency under the skiing mode with different step sizes.

6 CONCLUSION

In this research, a novel large-stroke planar motor driven by four piezo legs has been developed for nano-positioning applications. Its linear range of motion is limited only by the size of the base and its angular range of motion is up to 360° . There are three possible operation modes: the skiing mode, the stepping mode, and the tilting mode. The skiing mode provides the highest positioning speed for fast position adjustment. The stepping mode provides a high-accuracy trajectory tracking performance. The tilting mode offers the finest position control in 6-DOF. The above operation modes can also be combined to achieve both speed and accuracy in position control. For position feedback, an active planar encoder has been developed and integrated into the motion system for closed-loop position control. Experimental results demonstrate that the proposed planar motor can achieve nanometer level positioning resolution and large ranges of linear and angular motions with Omni-directional mobility.

Currently, the performance of the planar motor is limited by the performance of the encoder used. As a future work, we plan to further improve the measurement resolution and feed back speed of the active planar encoder to explore the true potential of this unique planar motor.

7 ACKNOWLEDGEMENT

The authors thank the National Science Foundation of China (NSFC) for the financial support of this work under grant No. 51375310.

REFERENCES

- [1] Shinno, Hidenori, et al. "X-Y- θ nano-positioning table system for a mother machine." *CIRP Annals-Manufacturing Technology* 53.1 (2004): 337-340.
- [2] Shinno, Hidenori, Hayato Yoshioka, and K. Taniguchi. "A newly developed linear motor-driven aerostatic XY planar motion table system for nano-machining." *CIRP Annals-Manufacturing Technology* 56.1 (2007): 369-372.

- [3] Dejima, Shuichi, et al. "Precision positioning of a five degree-of-freedom planar motion stage." *Mechatronics* 15.8 (2005): 969-987.
- [4] Lan, Hongbo, et al. "Review of the wafer stage for nanoimprint lithography." *Microelectronic Engineering* 84.4 (2007): 684-688.
- [5] Lee, Chang-Woo, and Seung-Woo Kim. "An ultraprecision stage for alignment of wafers in advanced microlithography." *Precision Engineering* 21.2 (1997): 113-122.
- [6] Sartori, S., and G. X. Zhang. "Geometric error measurement and compensation of machines." *CIRP Annals-Manufacturing Technology* 44.2 (1995): 599-609.
- [7] Kunzmann, H., T. Pfeifer, and J. Flügge. "Scales vs. laser interferometers performance and comparison of two measuring systems." *CIRP Annals-Manufacturing Technology* 42.2 (1993): 753-767.
- [8] Cao, Jiayong, et al. "A novel synchronous permanent magnet planar motor and its model for control applications." *Magnetics, IEEE Transactions on* 41.6 (2005): 2156-2163.
- [9] Gao, Wei, et al. "A surface motor-driven planar motion stage integrated with an XY θ _Z surface encoder for precision positioning." *Precision Engineering* 28.3 (2004): 329-337.
- [10] Ro, Seung-Kook, and Jong-Kweon Park. "A compact ultra-precision air bearing stage with 3-DOF planar motions using electromagnetic motors." *International Journal of Precision Engineering and Manufacturing* 12.1 (2011): 115-119.
- [11] Kim, Won-jong, and David L. Trumper. "High-precision magnetic levitation stage for photolithography." *Precision Engineering* 22.2 (1998): 66-77.
- [12] Li, Chaodong, Shi Xu, and Runfeng Liu. "P3M-2 Dynamic Analysis and Optimal Design of a Novel Small 2-D Planar Ultrasonic Motor." *Ultrasonics Symposium, 2006. IEEE. IEEE, 2006.*
- [13] Yan, Liang, et al. "A novel two degree-of-freedom ultrasonic planar motor driven by single stator." *Industrial Informatics (INDIN), 2012 10th IEEE International Conference on. IEEE, 2012.*
- [14] Ferreira, Antoine, Patrice Minotti, and Patrice Le Moal. "New multi-degree of freedom piezoelectric micromotors for micromanipulator applications." *Ultrasonics Symposium, 1995. Proceedings., 1995 IEEE. Vol. 1. IEEE, 1995.*
- [15] Kiyohiko Uozumi, Keiichi Nakamoto and Kageaki Fujioka. "Novel Three-Dimensional Positioner and Scanner for the STM Using Shear Deformation of Piezoceramic Plates." *Japanese Journal of Applied Physics*, Vol.27, No.1, January 1988, pp. L123-L126

- [16] Shamoto, Eiji, Hirokazu Murase, and Toshimichi Moriwaki. "Ultraprecision 6-axis table driven by means of walking drive." *CIRP Annals-Manufacturing Technology* 49.1 (2000): 299-302.
- [17] Shim, Jong-Youp, and Dae-Gab Gweon. "Piezo-driven metrological multiaxis nanopositioner." *Review of Scientific Instruments* 72.11 (2001): 4183-4187.
- [18] Juhas, L., et al. "A platform for micropositioning based on piezo legs." *Mechatronics* 11.7 (2001): 869-897.
- [19] Junbin Zhang, et al. "Large-stroke piezo-actuated planar motor for nanopositioning applications." *Proceedings of ASPE 2014 Annual Meeting* (2014): 105-110.

Figure Captions

Fig. 1. Design of the piezo-actuated planar motor (a) Overall design (b) Mechanical design of 1-DOF piezo leg (c) Mechanical design of 3-DOF piezo leg.

Fig. 2. Structural simulation result of the flexure fixed with the motion head. (a) Z -direction displacement under a force of 1N. (b) X -direction displacement under a force of 1N. (c) Motion simulation result of the motion head magnified by 200 times.

Fig. 3. Photos of the planar motor. (a) Bottom view. (b) Top view. (c) 1-DOF piezo leg. (d) 3-DOF piezo leg.

Fig. 4. Three operation modes. (a) Skiing mode. (b) Stepping mode. (c) Tilting mode.

Fig. 5. Definition of the coordinate systems.

Fig. 6. Definition of parameters and coordinate systems of the 3-DOF piezo leg.

Fig. 7. Control diagram of the planar motor system.

Fig. 8. System design of the active planar encoder (a) Planar motor integrated with the encoder. (b) $X1$ and $X2$ scanning area for calculating P_{X1} and P_{X2} . (c) $Y1$ scanning area for calculating P_{Y1} . (d) Converting the phase difference into displacement information.

Fig. 9. Coordinate systems definition of the active planar encoder.

Fig.10. Static stiffness and clamping force tests. (a) Stiffness test. (b) Clamping force test.

Fig.11. Tilting mode tests using a laser interferometer. (a) 5 nm step test along X -axis. (b) 0.02 arcsec step test about Z -axis.

Fig.12. Large-range motion performance (a) Position trajectory with a radius of 2 mm. (b) Angular trajectory with a sinusoidal curve of 5° amplitude.

Fig. 13. Planar motor speed vs. driving frequency under the skiing mode with different step sizes.